Computers and Structures 169 (2016) 57–68

Contents lists available at ScienceDirect

Computers and Structures

journal homepage: www.elsevier.com/locate/compstruc

The MITC4+ shell element and its performance

Yeongbin Ko [a], Phill-Seung Lee [a,*], Klaus-Jürgen Bathe [b]

[a] Department of Mechanical Engineering, Korea Advanced Institute of Science and Technology, 291 Daehak-ro, Yuseong-gu, Daejeon 34141, Republic of Korea
[b] Department of Mechanical Engineering, Massachusetts Institute of Technology, Cambridge, MA 02139, USA

ARTICLE INFO

Article history:
Received 9 December 2015
Accepted 3 March 2016

Keywords:
Shell structures
Shell finite elements
4-node element
MITC method
Convergence

ABSTRACT

The objective in this paper is to improve the performance of the 4-node MITC quadrilateral shell finite element, referred to as the MITC4 element (Dvorkin and Bathe, 1984). We propose a new MITC4 shell element, the MITC4+ element, in which the mid-surface membrane strain components are assumed using the concept of the MITC method. The tying membrane strains are obtained from four triangular domains which subdivide the mid-surface of the 4-node quadrilateral shell element. This approach alleviates locking that can happen when the MITC4 shell elements are geometrically distorted in curved geometries. Several basic tests including the isotropy, zero energy mode, and patch tests are performed. Through the solution of various shell problems, the convergence behavior of the MITC4+ shell element is studied to show the improvements reached.

1. Introduction

Shells are beautiful and efficient structures that exist in nature and many engineering applications, but their inherently complicated behavior is not easy to predict. The finite element method has been very useful for the analysis of shell structures. For several decades, the development of effective shell finite elements has been of great concern [1–17].

An "ideal" shell element should satisfy the ellipticity and consistency conditions [2,12–15]. In addition, an optimal uniform convergence behavior should be seen for any shell problem regardless of the asymptotic behavior (membrane-dominated, bending-dominated, and mixed shell behaviors) depending on the shell geometry, loading and boundary conditions [2,13,16]. It is extremely difficult to obtain an ideal shell finite element which gives for any problem an optimal uniform convergence behavior even when used in distorted meshes. Such element indeed does not exist yet.

To develop effective shell finite elements, the major challenge is to alleviate shear and membrane locking that seriously deteriorate the solution accuracy in bending-dominated and membrane-bending mixed shell problems [5,13,16]. Unlike shear locking, membrane locking occurs only when the shell element geometry is curved. Membrane locking has been treated quite successfully for higher order shell elements [6,9,17].

The MITC (Mixed Interpolation of Tensorial Components) method was first developed to reduce shear locking for the 4-node continuum mechanics based MITC4 shell element [1]. Then, the method has been successfully used to reduce both shear and membrane locking in higher order quadrilateral and triangular shell finite elements (the MITC9, MITC16 and MITC6 shell elements) [5–8]. However, in the MITC4 element formulation, the membrane strains are not modified (because the element is usually relatively flat in its geometry). This can lead to some membrane locking when curved geometries are solved with distorted meshes.

The membrane locking phenomenon has been well studied in 3-node curved beam and 9-node shell elements, for which various methodologies have been proposed to reduce the locking [6,18–20]. However, there have been few attempts to improve 4-node quadrilateral shell elements [21–25] by modifying the membrane strain components. Such modifications resulted into not satisfying the patch and/or zero energy mode tests, and to severely deteriorating the in-plane behaviors of 4-node shell elements. For those reasons, the previous attempts to improve 4-node quadrilateral shell elements have not been successful.

In this paper, we propose a new assumed membrane strain field for the MITC4 shell element, which is simple and effective for reducing locking but the membrane behavior is well preserved. The key idea is to construct the assumed membrane strain field by utilizing the membrane strains obtained from four triangular subdomains representing the 4-node quadrilateral shell element. The shear locking is treated as in the original MITC4 shell element formulation.

* Corresponding author.
E-mail address: phillseung@kaist.edu (P.S. Lee).

http://dx.doi.org/10.1016/j.compstruc.2016.03.002
0045-7949/

In the following sections, the formulation of the MITC4 shell element is briefly reviewed and then the formulation of the new MITC4+ shell element is given. The performance of the new element is presented through basic numerical tests and convergence tests.

2. The MITC4 shell finite element

In this section, we briefly review the formulation of the MITC4 shell element.

The geometry of a standard 4-node continuum mechanics based quadrilateral shell finite element is interpolated using [1,12]

$$\mathbf{x}(r,s,t)=\sum_{i=1}^{4}h_i(r,s)\mathbf{x}_i+\frac{t}{2}\sum_{i=1}^{4}a_i h_i(r,s)\,\mathbf{V}_n^i, \tag{1}$$

where $h_i(r,s)$ is the two-dimensional interpolation function of the standard isoparametric procedure corresponding to node i, $\mathbf{x}_i$ is the position vector of node i in the global Cartesian coordinate system, and a_i and $\mathbf{V}_n^i$ denote the shell thickness and the director vector at the node, see Fig. 1.

The corresponding displacement interpolation of the element is

$$\mathbf{u}(r,s,t)=\sum_{i=1}^{4}h_i(r,s)\mathbf{u}_i+\frac{t}{2}\sum_{i=1}^{4}a_i h_i(r,s)\,(-\mathbf{V}_2^i\alpha_i+\mathbf{V}_1^i\beta_i), \tag{2}$$

in which $\mathbf{u}_i$ is the nodal displacement vector in the global Cartesian coordinate system, $\mathbf{V}_1^i$ and $\mathbf{V}_2^i$ are unit vectors orthogonal to $\mathbf{V}_n^i$ and to each other, and α_i and β_i are the rotations of the director vector $\mathbf{V}_n^i$ about $\mathbf{V}_1^i$ and $\mathbf{V}_2^i$, respectively, at node i .

The linear terms of the displacement-based covariant strain components are given by

$$e_{ij}=\frac{1}{2}(\mathbf{g}_i\cdot\mathbf{u}_{,j}+\mathbf{g}_j\cdot\mathbf{u}_{,i}), \tag{3}$$

in which

$$\mathbf{g}_i=\frac{\partial\mathbf{x}}{\partial r_i},\quad \mathbf{u}_{,i}=\frac{\partial\mathbf{u}}{\partial r_i}\qquad \text{with}\quad r_1=r,\ r_2=s,\ r_3=t. \tag{4}$$

For the MITC4 shell element, the covariant in-plane strain components are calculated using Eqs. (1)–(3) without any modification. The transverse shear strain field is based on assuming constant covariant transverse shear strain conditions along the edges, see Ref. [1]

$$\tilde{e}_{rt}=\frac{1}{2}(1+s)e_{rt}^{(A)}+\frac{1}{2}(1-s)e_{rt}^{(B)},$$
$$\tilde{e}_{st}=\frac{1}{2}(1+r)e_{st}^{(C)}+\frac{1}{2}(1-r)e_{st}^{(D)}, \tag{5}$$

where the tying points are shown in Fig. 2 [1,9].

3. The MITC4+ shell finite element

In the formulation of the new 4-node shell element the mid-surface of the element is subdivided into four non-overlapping 3-node triangular domains, and the assumed membrane strain field is constructed using the membrane strains of the flat triangular domains. The geometry and displacement interpolations of the new shell elements are as for the MITC4 shell element.

We can write the covariant in-plane strain in Eq. (3) as

$$e_{ij}=e_{ij}^{m}+t\,e_{ij}^{b1}+t^2e_{ij}^{b2}\quad\text{with}\quad i,j=1,\ 2, \tag{6a}$$

$$e_{ij}^{m}=\frac{1}{2}\left(\frac{\partial\mathbf{x}_m}{\partial r_i}\cdot\frac{\partial\mathbf{u}_m}{\partial r_j}+\frac{\partial\mathbf{x}_m}{\partial r_j}\cdot\frac{\partial\mathbf{u}_m}{\partial r_i}\right), \tag{6b}$$

$$e_{ij}^{b1}=\frac{1}{2}\left(\frac{\partial\mathbf{x}_m}{\partial r_i}\cdot\frac{\partial\mathbf{u}_b}{\partial r_j}+\frac{\partial\mathbf{x}_m}{\partial r_j}\cdot\frac{\partial\mathbf{u}_b}{\partial r_i}+\frac{\partial\mathbf{x}_b}{\partial r_i}\cdot\frac{\partial\mathbf{u}_m}{\partial r_j}+\frac{\partial\mathbf{x}_b}{\partial r_j}\cdot\frac{\partial\mathbf{u}_m}{\partial r_i}\right), \tag{6c}$$

$$e_{ij}^{b2}=\frac{1}{2}\left(\frac{\partial\mathbf{x}_b}{\partial r_i}\cdot\frac{\partial\mathbf{u}_b}{\partial r_j}+\frac{\partial\mathbf{x}_b}{\partial r_j}\cdot\frac{\partial\mathbf{u}_b}{\partial r_i}\right), \tag{6d}$$

with

$$\mathbf{x}_m=\sum_{i=1}^{4}h_i(r,s)\mathbf{x}_i,\quad \mathbf{x}_b=\frac{1}{2}\sum_{i=1}^{4}a_i h_i(r,s)\,\mathbf{V}_n^i,$$

$$\mathbf{u}_m=\sum_{i=1}^{4}h_i(r,s)\mathbf{u}_i,\quad \mathbf{u}_b=\frac{1}{2}\sum_{i=1}^{4}a_i h_i(r,s)\,(-\mathbf{V}_2^i\alpha_i+\mathbf{V}_1^i\beta_i), \tag{7}$$

in which the first term e_{ij}^{m} is the covariant in-plane membrane strain at the shell mid-surface ($t=0$), and the remaining terms are the covariant in-plane strains due to bending. The membrane strain in

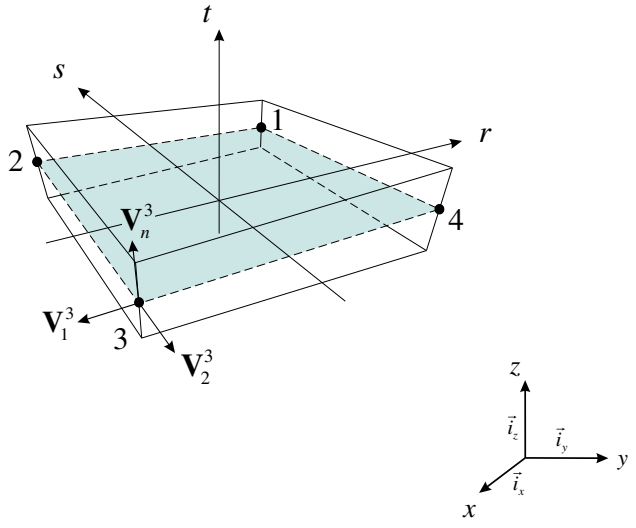

Fig. 1. A standard 4-node quadrilateral continuum mechanics based shell finite element.

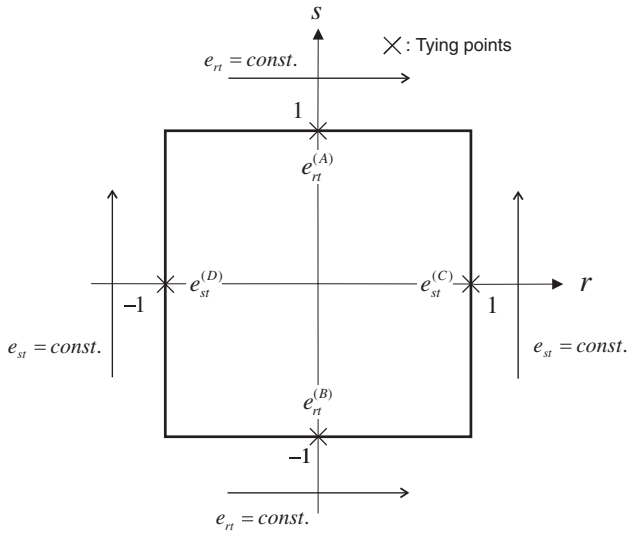

Fig. 2. Tying positions (A), (B), (C) and (D) for the assumed transverse shear strain field of the MITC4 shell element. The constant transverse shear strain conditions are imposed along its edges.

Eq. (6b) can induce locking in general, and since this locking results from a membrane component, it is referred to as "membrane locking".

Let us define the center point denoted by '5' in the mid-surface of the 4-node shell element as shown in Fig. 3

$$\mathbf{x}_5 = \sum_{i=1}^{4} \gamma_i \mathbf{x}_i, \tag{8}$$

where the constants γ_i are used to determine the position of the center point. The choice of constants is important for the element isotropy and the membrane patch tests.

In this study, the constants in Eq. (8) are determined using the following equation (for the detailed derivation, see Appendix A)

$$\begin{aligned}[\gamma_1 \quad \gamma_2 \quad \gamma_3 \quad \gamma_4] = &\frac{1}{2}\frac{A_1}{A_1+A_2}\left[\tfrac{1}{3} \quad \tfrac{1}{3} \quad 0 \quad \tfrac{1}{3}\right] + \frac{1}{2}\frac{A_2}{A_1+A_2}\left[0 \quad \tfrac{1}{3} \quad \tfrac{1}{3} \quad \tfrac{1}{3}\right] \\ &+ \frac{1}{2}\frac{A_3}{A_3+A_4}\left[\tfrac{1}{3} \quad \tfrac{1}{3} \quad \tfrac{1}{3} \quad 0\right] + \frac{1}{2}\frac{A_4}{A_3+A_4}\left[\tfrac{1}{3} \quad 0 \quad \tfrac{1}{3} \quad \tfrac{1}{3}\right],\end{aligned} \tag{9}$$

where A_1, A_2, A_3 and A_4 are the areas of triangles 1, 2, 3, and 4 shown in Fig. 4. The center point is located at the mean position of two geometric centroids in Fig. 4. When the geometry of the 4-node shell element is flat, the center point obtained using Eqs. (8) and (9) is located at the centroid of the mid-surface of the 4-node shell element.

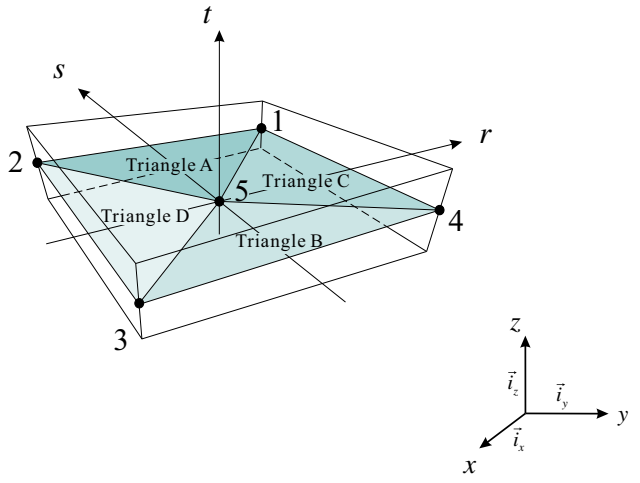

Fig. 3. Triangular subdivision of the mid-surface of the 4-node shell element.

Using the defined center point, we divide the mid-surface of the 4-node shell element into four flat triangular domains, see Fig. 3. Each triangular domain can be interpolated using the following geometry interpolation function

$$\widehat{\mathbf{x}}(r,s,t) = \sum_{i=1}^{3} \widehat{h}_i(r,s)\widehat{\mathbf{x}}_i \quad \text{with} \quad \widehat{h}_1(r,s) = r, \ \widehat{h}_2(r,s) = s, \ \widehat{h}_3(r,s) = 1 - r - s, \tag{10}$$

and

$$\begin{aligned}&\widehat{\mathbf{x}}_1 = \mathbf{x}_1, \ \widehat{\mathbf{x}}_2 = \mathbf{x}_2, \ \widehat{\mathbf{x}}_3 = \mathbf{x}_5 \quad \text{for triangle A,} \\ &\widehat{\mathbf{x}}_1 = \mathbf{x}_3, \ \widehat{\mathbf{x}}_2 = \mathbf{x}_4, \ \widehat{\mathbf{x}}_3 = \mathbf{x}_5 \quad \text{for triangle B,} \\ &\widehat{\mathbf{x}}_1 = \mathbf{x}_4, \ \widehat{\mathbf{x}}_2 = \mathbf{x}_1, \ \widehat{\mathbf{x}}_3 = \mathbf{x}_5 \quad \text{for triangle C,} \\ &\widehat{\mathbf{x}}_1 = \mathbf{x}_2, \ \widehat{\mathbf{x}}_2 = \mathbf{x}_3, \ \widehat{\mathbf{x}}_3 = \mathbf{x}_5 \quad \text{for triangle D,}\end{aligned}$$

in which $\widehat{h}_i(r,s)$ is the two-dimensional interpolation function of the 3-node triangular element corresponding to node i, and $\widehat{\mathbf{x}}_i$ is the position vector at node i. Note that the subdivision into two non-overlapping triangular domains is also possible, but then the element isotropy cannot be satisfied.

The interpolation of the corresponding translational displacement vector is given by

$$\widehat{\mathbf{u}}(r,s,t) = \sum_{i=1}^{3} \widehat{h}_i(r,s)\widehat{\mathbf{u}}_i, \tag{11}$$

where $\widehat{\mathbf{u}}_i$ is the translational displacement vector at node i .

In the MITC4+ shell element, the displacement vector at the center point is represented by the displacement vectors at the corner nodes

$$\mathbf{u}_5 = \sum_{i=1}^{4} \gamma_i \mathbf{u}_i. \tag{12}$$

Note that the isoparametric relation between Eqs. (8) and (12) is important to correctly represent rigid body modes in the 4-node shell element. Note that the displacements at the center point are not degrees of freedom in the element formulation.

The covariant membrane strain in the triangular domains is given by

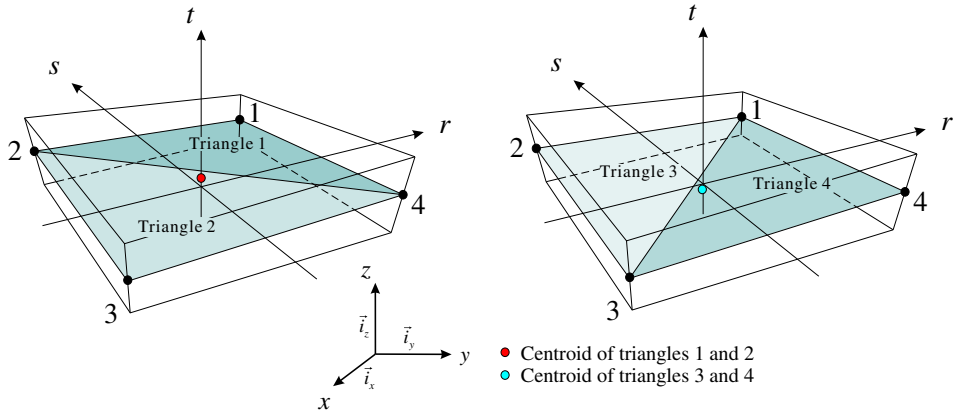

Fig. 4. Four triangles to determine the center point of the MITC4+ shell element.

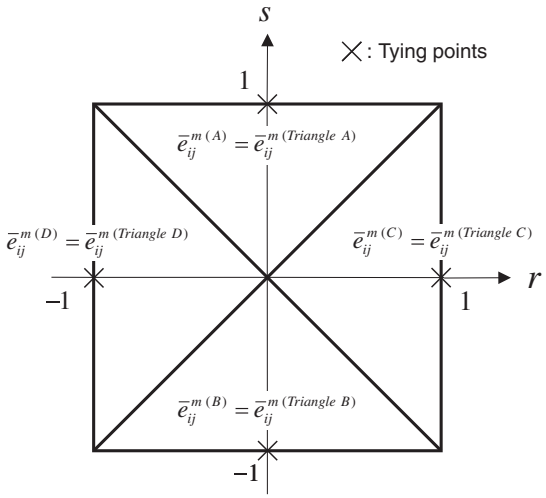

$$\tilde{e}_{ij}^{m} = a + br + cs + drs$$

$$a = \frac{1}{4}(\bar{e}_{ij}^{m(A)} + \bar{e}_{ij}^{m(B)} + \bar{e}_{ij}^{m(C)} + \bar{e}_{ij}^{m(D)})$$

$$b = \frac{1}{2}(-\bar{e}_{ij}^{m(D)} + \bar{e}_{ij}^{m(C)})$$

$$c = \frac{1}{2}(-\bar{e}_{ij}^{m(B)} + \bar{e}_{ij}^{m(A)})$$

$$d = 0$$

Fig. 5. Tying positions (A), (B), (C) and (D) for the assumed membrane strain field of the MITC4+ shell element.

$$\widehat{e}_{ij}^{m} = \frac{1}{2}\left(\frac{\partial \widehat{\mathbf{x}}}{\partial r_i}\cdot\frac{\partial \widehat{\mathbf{u}}}{\partial r_j} + \frac{\partial \widehat{\mathbf{x}}}{\partial r_j}\cdot\frac{\partial \widehat{\mathbf{u}}}{\partial r_i}\right) \quad \text{with} \quad i,j = 1,2. \tag{13}$$

The covariant membrane strain in Eq. (13) has two covariant base vectors,

$$\widehat{\mathbf{g}}_i = \frac{\partial \widehat{\mathbf{x}}}{\partial r_i} \quad \text{with} \quad i = 1,2, \tag{14a}$$

which are supplemented with the third covariant base vector of

$$\widehat{\mathbf{g}}_3 = \mathbf{g}_3. \tag{14b}$$

In order to apply the assumed strain method, the covariant membrane strain from each triangular domain must be transported to the natural coordinate system of the 4-node shell element. The strain transformation is given by ($i,j = 1,2$ and $k,l = 1,2$),

$$\bar{e}_{ij}^{m} = \widehat{e}_{kl}^{m}(\mathbf{g}_i \cdot \widehat{\mathbf{g}}^k)(\mathbf{g}_j \cdot \widehat{\mathbf{g}}^l), \tag{15}$$

in which $\widehat{\mathbf{g}}^i \cdot \widehat{\mathbf{g}}_j = \delta_{ij}$ with δ_{ij} the Kronecker delta.

Using the covariant membrane strains evaluated from the four triangular domains, we need to construct a new assumed strain field which alleviates the locking. We start from the following equation

$$\tilde{e}_{ij}^{m} = a + br + cs + drs \quad \text{with} \quad i,j = 1,2, \tag{16}$$

in which the coefficients a, b, c and d are determined using the covariant membrane strains evaluated in the triangular domains.

While the strains are constant within each triangular domain, we choose the tying positions to be symmetric about the element center, as shown in Fig. 5, We then use the following tying conditions

$$\begin{aligned} &\tilde{e}_{ij}^{m}(0,1) = \bar{e}_{ij}^{m(A)}, \quad \tilde{e}_{ij}^{m}(0,-1) = \bar{e}_{ij}^{m(B)}, \\ &\tilde{e}_{ij}^{m}(1,0) = \bar{e}_{ij}^{m(C)}, \quad \tilde{e}_{ij}^{m}(-1,0) = \bar{e}_{ij}^{m(D)}, \end{aligned} \tag{17}$$

The four coefficients in Eq. (16) are thus obtained as

$$\begin{aligned} &a = \frac{1}{4}(\bar{e}_{ij}^{m(A)} + \bar{e}_{ij}^{m(B)} + \bar{e}_{ij}^{m(C)} + \bar{e}_{ij}^{m(D)}), \quad b = \frac{1}{2}\left(-\bar{e}_{ij}^{m(D)} + \bar{e}_{ij}^{m(C)}\right), \\ &c = \frac{1}{2}\left(-\bar{e}_{ij}^{m(B)} + \bar{e}_{ij}^{m(A)}\right), \\ &d = 0. \end{aligned} \tag{18}$$

Finally, the new assumed strain field for the membrane strains is given as

$$\begin{aligned} \tilde{e}_{ij}^{m} = {} & \frac{1}{4}(\bar{e}_{ij}^{m(A)} + \bar{e}_{ij}^{m(B)} + \bar{e}_{ij}^{m(C)} + \bar{e}_{ij}^{m(D)}) + \frac{1}{2}\left(-\bar{e}_{ij}^{m(D)} + \bar{e}_{ij}^{m(C)}\right)r \\ & + \frac{1}{2}\left(-\bar{e}_{ij}^{m(B)} + \bar{e}_{ij}^{m(A)}\right)s, \end{aligned} \tag{19}$$

Note that the assumed membrane strains in Eq. (19) do not have the bi-linear term (rs) which causes membrane locking of the MITC4 element when geometrically distorted.

As for the MITC4 element, we use $2 \times 2 \times 2$ Gauss integration over the (distorted) original element shape to evaluate the stiffness matrix of the MITC4+ shell element.

The assumed membrane strain field in Eq. (19) can be directly adopted in the 4-node shell element without considering the triangular subdivision used in this study. Then, while the convergence behavior is similar to the behavior of the MITC4+ shell element, the resulting element largely fails the membrane patch test.

4. Remarks on previous studies

In this section, we briefly comment on some previous attempts to resolve membrane locking of 4-node shell elements.

Membrane locking of 4-node shell elements can be greatly alleviated using the well-known reduced integration [21–23]. Such elements suffer from rank deficiency and do not properly represent physical rigid body modes; thus appropriate stabilization and displacement projection techniques need be used [21–23]. The elements may be useful for some applications, but the use of stabilization factors is undesirable and the membrane and perhaps bending predictions are not optimal.

There have been some attempts to use the assumed strain method, or similar techniques, see Refs. [24–26]. In Ref. [24], the discrete strain gap method was employed to reduce membrane locking, but the resulting element was not effective.

Choi and Paik [25] successfully alleviated the membrane locking of a 4-node shell element and achieved good in-plane behaviors using the following assumed strain field

$$\tilde{e}_{11}^{m} = \frac{1}{2}\left(e_{11}^{m(B)} + e_{11}^{m(A)}\right) + \frac{1}{2}(-e_{11}^{m(B)} + e_{11}^{m(A)})s, \tag{20a}$$

$$\tilde{e}_{22}^{m} = \frac{1}{2}(e_{22}^{m(D)} + e_{22}^{m(C)}) + \frac{1}{2}\left(-e_{22}^{m(D)} + e_{22}^{m(C)}\right)r, \tag{20b}$$

$$\tilde{e}_{12}^{m} = \frac{1}{4}\left(e_{12}^{m(A)} + e_{12}^{m(B)} + e_{12}^{m(C)} + e_{12}^{m(D)}\right), \tag{20c}$$

where the tying points are shown in Fig. 5. However, the element largely fails the membrane patch test.

In Ref. [26], the author used the QMITC membrane element [27] to represent the in-plane behavior of the MITC4 shell element. This is a valuable approach but the element is rather costly computationally.

In addition, all these elements have not been tested thoroughly using strong benchmark problems and distorted meshes.

5. Basic numerical tests

Here, basic numerical tests are conducted to examine the MITC4+ shell element. We first consider the isotropy, patch and zero energy mode tests. We also test the membrane behavior of the element through the solution of Cook's problem to check whether the membrane performance deteriorates compared to the MITC4 shell element.

As in triangular shell elements, spatially isotropic behavior is an important requirement for quadrilateral shell elements. The element behavior should not depend on the sequence of node numbering, i.e. the element orientation [2–4,8]. The MITC4+ shell element passes this test.

We perform three patch tests: the membrane, bending and shearing patch tests, see Refs. [1–4,8,13,17,28] for the patch tests. The geometry, mesh, loading and boundary conditions are shown in Fig. 6. The patch of elements is subjected to the minimum number of constrains to prevent rigid body motions and the nodal point forces on the boundary corresponding to the constant stress states are applied. If the constant stress fields are calculated, the patch tests are passed. The MITC4+ shell element exactly passes the shear and bending patch tests. The results of the membrane patch test are shown in Fig. 7. The new element practically also passes the membrane patch test, similar to the MITC9 shell element.

In the zero energy mode tests, the number of zero eigenvalues of the stiffness matrix of a single unsupported element are counted [1–4,8,13,17,28]. For the MITC4+ shell element, only the six zero eigenvalues corresponding to the six rigid body modes are obtained. That is, the MITC4+ shell element passes the zero energy mode test.

In order to test the in-plane bending and shearing behaviors of the MITC4+ shell element, Cook's problem shown in Fig. 8 is considered [29,30]. The vertical displacement at tip A should converge to the reference solution as the mesh is refined. Table 1 presents the tip displacements obtained using the MITC4+ and MITC4 shell elements. Both elements show a similar performance and converge to the reference solution. This numerical test shows that the in-plane behavior of the MITC4+ shell element is not worse than the behavior of the MITC4 shell element.

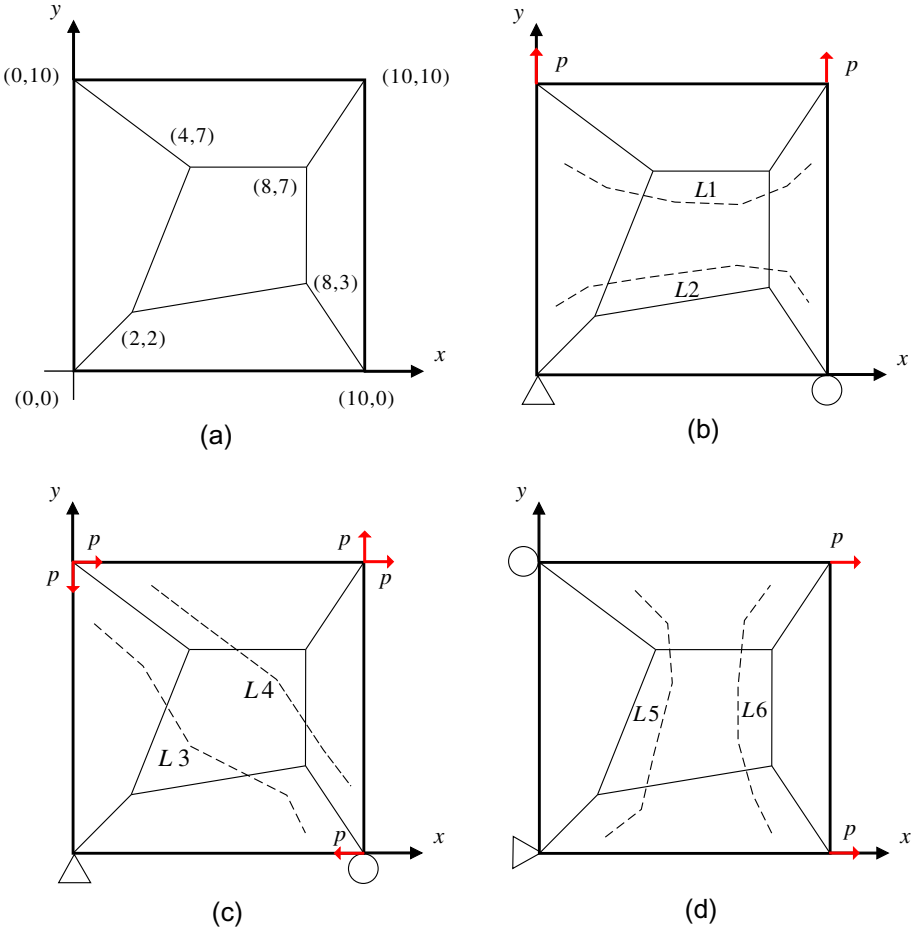

Fig. 6. Mesh geometry used for the membrane patch tests is shown in (a). Loading and boundary conditions and the lines through element Gauss points for stress evaluation are shown in (b)–(d) ($p = 1.0$, thickness = 1.0, $E = 2.1 \times 10^6$, $\nu = 0.3$).

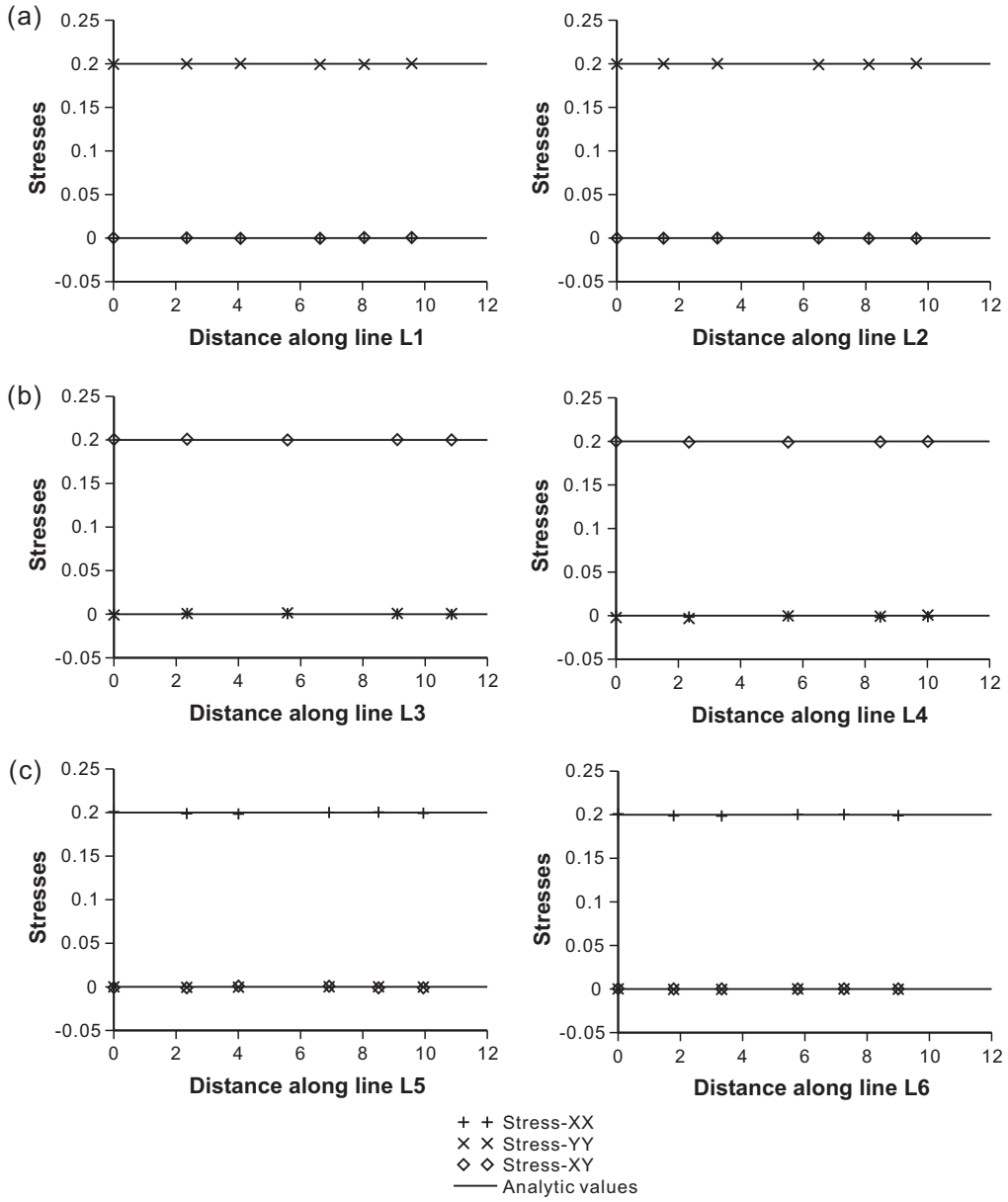

Fig. 7. Stresses along lines L1–L6 for the membrane patch tests of the MITC4 + shell element. Results of the patch tests in Fig. 6(b)–(d) are shown in (a)–(c), respectively.

6. Convergence studies

In this section, we perform convergence studies using well-established benchmark problems to study the behavior of shell elements: a clamped square plate problem, cylindrical shell problems, and hyperboloid shell problems [2–5,7,8,13,31–35]. We aim to measure the solution errors in an appropriate norm considering membrane and bending-dominated shell problems with various curvatures, thicknesses, and boundary conditions.

To measure the error in the finite element solution, we use the s-norm proposed by Hiller and Bathe [32]

$$\|\mathbf{u}-\mathbf{u}_h\|_s^2 = \int_\Omega \Delta\boldsymbol{\varepsilon}^T \Delta\boldsymbol{\tau} d\Omega \quad \text{with} \quad \Delta\boldsymbol{\varepsilon} = \boldsymbol{\varepsilon} - \boldsymbol{\varepsilon}_h, \Delta\boldsymbol{\tau} = \boldsymbol{\tau} - \boldsymbol{\tau}_h, \tag{21}$$

where $\mathbf{u}$ is the exact solution, $\mathbf{u}_h$ is the solution of the finite element discretization, and $\boldsymbol{\varepsilon}$ and $\boldsymbol{\tau}$ are the strain and stress vectors. This is a proper norm for investigating whether the finite element formulation satisfies the consistency and inf-sup conditions [5,11,14,32].

Since many good benchmark shell problems designed to detect locking have no analytical solution, an accurate finite element solution using a very fine mesh $\mathbf{u}_{ref}$ is used to replace the exact solution $\mathbf{u}$. Hence the s-norm in Eq. (21) is modified to be

$$\|\mathbf{u}_{ref}-\mathbf{u}_h\|_s^2 = \int_{\Omega_{ref}} \Delta\boldsymbol{\varepsilon}^T \Delta\boldsymbol{\tau} d\Omega_{ref} \quad \text{with} \quad \Delta\boldsymbol{\varepsilon} = \boldsymbol{\varepsilon}_{ref} - \boldsymbol{\varepsilon}_h, \Delta\boldsymbol{\tau} = \boldsymbol{\tau}_{ref} - \boldsymbol{\tau}_h. \tag{22}$$

To study the solution convergence of shell finite elements with decreasing thicknesses, we use the normalized relative error E_h

$$E_h = \frac{\|\mathbf{u}_{ref}-\mathbf{u}_h\|_s^2}{\|\mathbf{u}_{ref}\|_s^2}. \tag{23}$$

The theoretical convergence behavior, which corresponds to the optimal convergence, is given by

$$E_h \cong Ch^k, \tag{24}$$

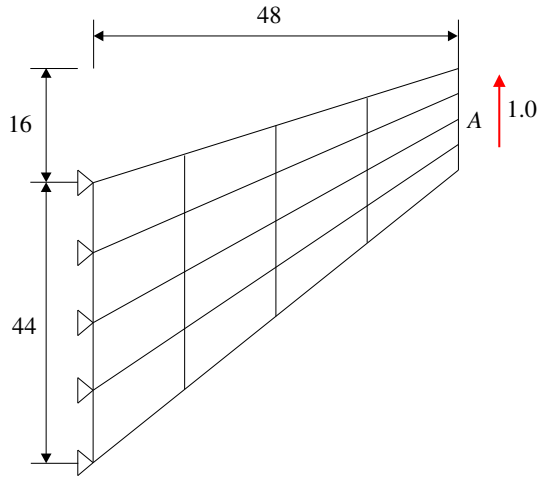

Fig. 8. Cook's problem. Plane stress condition is considered with $E = 1.0$ and $\nu = 1/3$.

Table 1
Vertical displacements at the center of tip A for Cook's problem. The reference value is 23.9642.

Elements	Mesh				
	2×2	4×4	8×8	16×16	32×32
MITC4	11.8452	18.2992	22.0792	23.4304	23.8176
MITC4+	11.7291	18.2662	22.0751	23.4301	23.8176

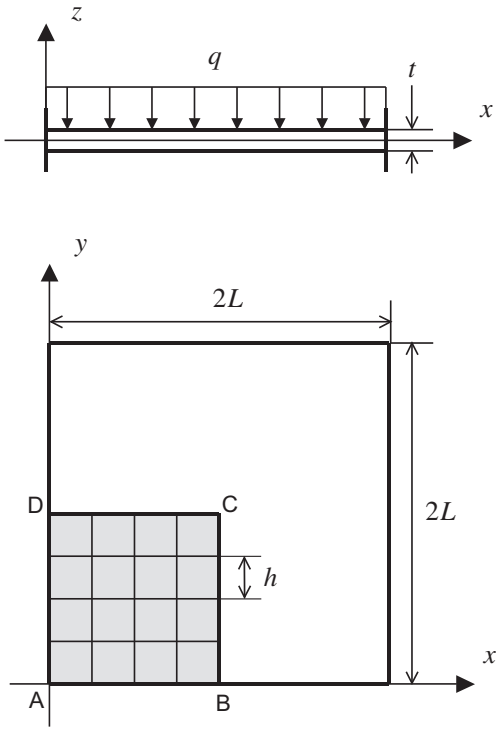

Fig. 9. Fully clamped square plate under uniform pressure ($L = 1.0$, $E = 1.7472 \times 10^7$, $q = 1.0$ and $\nu = 0.3$).

in which C is a constant independent of the shell thickness and h is the element size. For 4-node shell elements, $k = 2$.

In this study, well-converged reference solutions calculated using fine meshes of the MITC9 shell elements are used. The MITC9 shell element is known to satisfy the ellipticity and consistency conditions and to show good convergence behavior [5,32,33].

6.1. Fully clamped square plate problem

The plate bending problem [2–4,7,8,33,35] shown in Fig. 9 is considered. A square plate of dimensions $2L \times 2L$ and uniform thickness t is subjected to a uniform pressure. Utilizing the symmetry condition, only a one-quarter model is considered, with the following boundary conditions: $u_x = \theta_y = 0$ along BC, $u_y = \theta_x = 0$ along DC and $u_x = u_y = u_z = \theta_x = \theta_y = 0$ along AB and AD. In addition to the regular mesh in Fig. 9, we consider the same plate bending problem with distorted meshes shown in Fig. 10. Then, when we use an $N \times N$ element mesh, each edge is discretized in the following ratio: L_1: L_2: L_3: ... L_N = 1: 2: 3: ... N.

Fig. 11 gives the convergence curves of the MITC4 and MITC4+ shell elements. A 72×72 element mesh of the MITC9 shell element is used to obtain the reference solution. We use $N \times N$ element meshes (N = 4, 8, 16, 32, and 64) to calculate the solutions. The element size in the convergence curves is $h = L/N$. The performance of the elements is uniformly optimal in both the regular and distorted meshes. Note that membrane locking is inherently not present in this plate bending problem.

6.2. Cylindrical shell problems

We consider the cylindrical shell of length $2L$, radius R and uniform thickness t as shown in Fig. 12, see Refs. [2–4,8,31]. The loading is a smoothly varying pressure $p(\theta)$

$$p(\theta) = p_0 \cos(2\theta). \tag{25}$$

This shell structure shows two different asymptotic behaviors depending on the boundary conditions at its ends: bending-dominated behavior when both ends are free and membrane-dominated behavior when both ends are clamped.

Using symmetry, only the region ABCD in Fig. 12 is modeled. For the membrane-dominated problem, the clamped boundary condition is imposed: $u_x = \beta = 0$ along BC, $u_y = \alpha = 0$ along DC, $u_z = \alpha = 0$ along AB, and $u_x = u_y = u_z = \alpha = \beta = 0$ along AD. For the bending-dominated problem, the free boundary condition is imposed: $u_x = \beta = 0$ along BC, $u_y = \alpha = 0$ along DC, and $u_z = \alpha = 0$ along AB. When using the clamped boundary condition, the regular mesh is graded with a boundary layer of width $2\sqrt{t}$, see Refs. [11,31] for details. In the free boundary condition, the graded

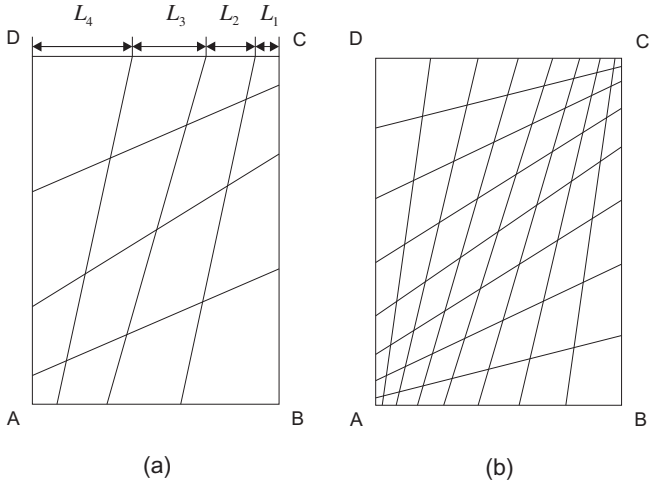

Fig. 10. Distorted mesh patterns for (a) $N = 4$ and (b) $N = 8$.

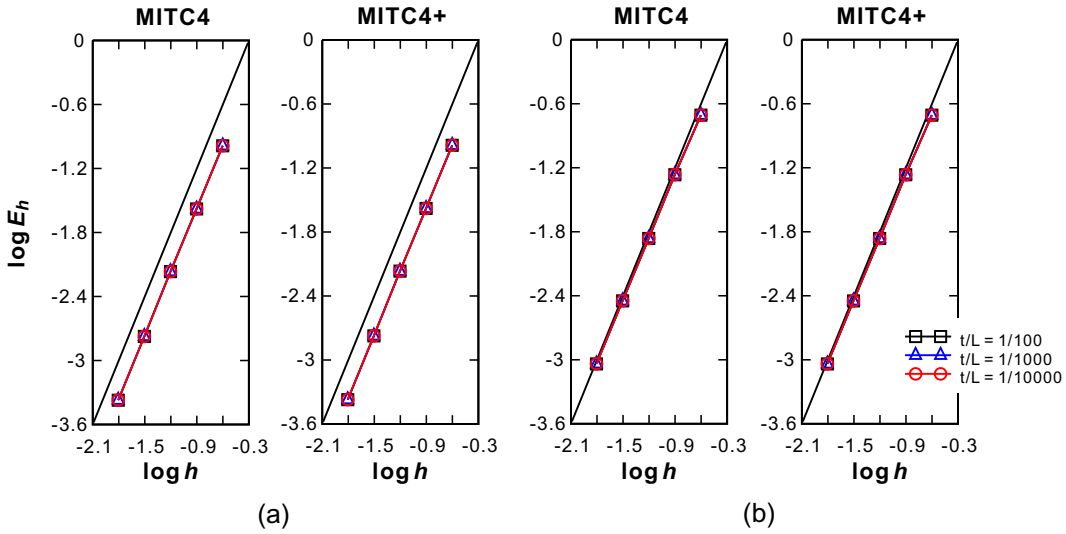

Fig. 11. Convergence curves for the fully clamped square plate problem with (a) the regular and (b) distorted meshes shown in Fig. 10. The bold line represents the optimal convergence rate.

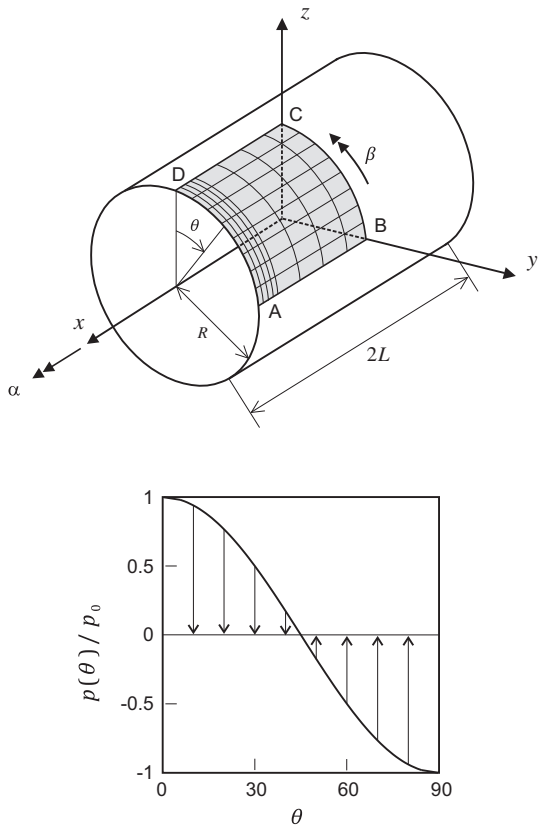

Fig. 12. Cylindrical shell problem (8×8 regular mesh, $L = R = 1.0$, $E = 2.0 \times 10^5$, $\nu = 1/3$ and $p_0 = 1.0$).

mesh with a boundary layer of width $0.5\sqrt{t}$ is considered. We also perform the convergence studies with the distorted meshes shown in Fig. 10.

Fig. 13 gives the convergence curves of the MITC4 and MITC4+ shell elements for the clamped cylindrical shell problems. The reference solutions are calculated using a 72×72 element mesh of MITC9 shell elements. The solutions are obtained with $N \times N$ element meshes ($N = 4$, 8, 16, 32, and 64). The element size is $h = L/N$. In this problem, both shell elements present similarly good convergence behaviors.

Fig. 14 shows the convergence curves for the free cylindrical shell problems. Note that, in the regular meshes, all 4-node shell elements have a flat geometry, and thus membrane locking does not occur. However, in the distorted meshes, the element geometry is not flat, which induces membrane locking. In those cases, the performance of the MITC4 shell element severely deteriorates. The MITC4+ shell element shows a significantly improved performance compared to the MITC4 shell element.

6.3. Hyperboloid shell problems

Finally, the hyperboloid shell shown in Fig. 15(a) is considered, see Refs. [2–5,8,32,34]. The mid-surface of the shell structure is given by

$$x^2 + z^2 = 1 + y^2; \quad y \in [-1, \quad 1]. \tag{26}$$

As for the cylindrical shell problems, a smoothly varying pressure in Fig. 12 is applied,

$$p(\theta) = p_0 \cos(2\theta). \tag{27}$$

A bending-dominated behavior is obtained with free ends and a membrane-dominated behavior is given with clamped ends, similar to the cases of the cylindrical shell.

Due to symmetry, only one-eighth of the structure corresponding to the shaded region ABCD in Fig. 15(a) is modeled for the analysis. For the membrane-dominated case, the clamped boundary condition is imposed: $u_z = \beta = 0$ along BC, $u_x = \beta = 0$ along AD, and $u_y = \alpha = 0$ along DC, and $u_x = u_y = u_z = \alpha = \beta = 0$ along AB. For the bending-dominated case, the free boundary condition is imposed: $u_z = \beta = 0$ along BC, $u_x = \beta = 0$ along AD, and $u_y = \alpha = 0$ along DC.

In both cases, a 72×72 element mesh of MITC9 shell elements is used to obtain the reference solutions. The solutions are calculated using $N \times N$ element meshes ($N = 4$, 8, 16, 32 and 64). The element size is $h = L/N$. For the clamped boundary condition, the regular mesh graded in a boundary layer of width $6\sqrt{t}$ shown in Fig. 15(b) is considered, see Refs. [5,11,32]. For the free boundary condition, the regular mesh is graded in a boundary layer of width $0.5\sqrt{t}$ [11,32]. We also perform the convergence studies with the distorted meshes shown in Fig. 10.

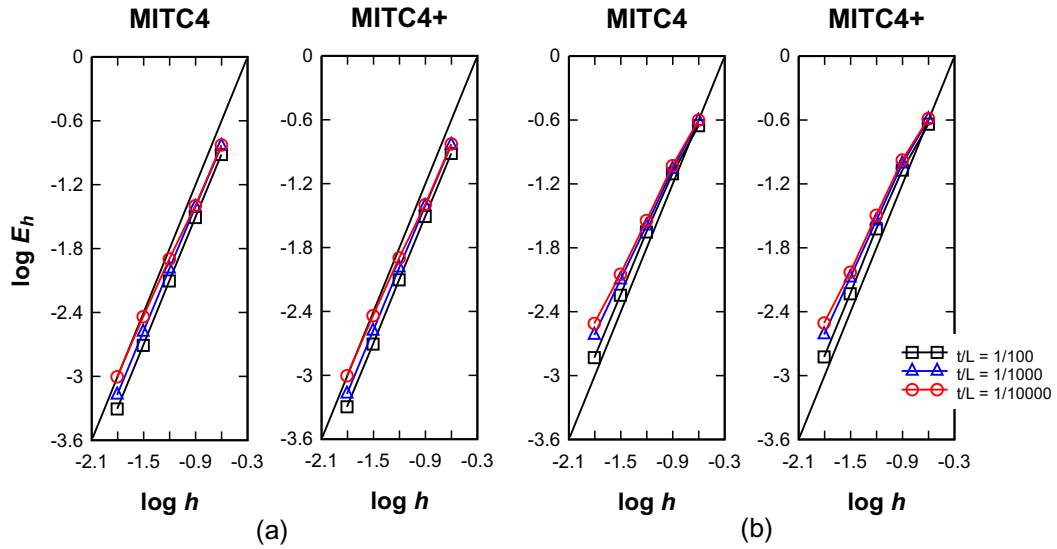

Fig. 13. Convergence curves for the clamped cylindrical shell problem with (a) the regular or (b) distorted meshes shown in Fig. 10. The bold line represents the optimal convergence rate.

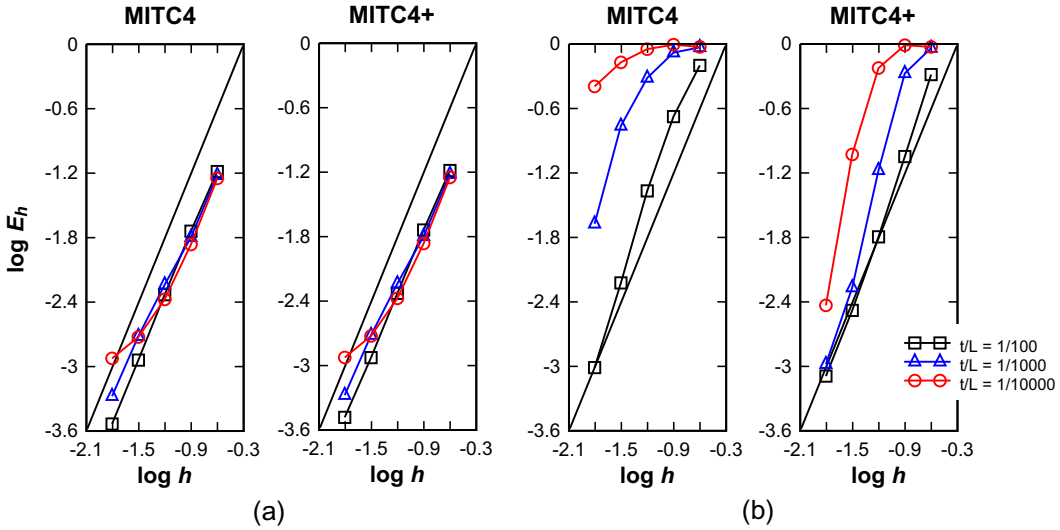

Fig. 14. Convergence curves for the free cylindrical shell problem with (a) the regular and (b) distorted meshes shown in Fig. 10. The bold line represents the optimal convergence rate.

Fig. 16 shows the good convergence behavior of the MITC4 and MITC4+ shell elements for the clamped hyperboloid shell problem. Fig. 17 shows the convergence curves for the free hyperboloid shell problem. While both shell elements behave well in the regular meshes, the convergence deteriorates when using the distorted meshes. However, the MITC4+ shell element shows a significantly improved performance compared to the MITC4 shell element.

In Figs. 18 and 19, we finally present the distributions of membrane strain components obtained using the MITC4 and MITC4+ shell elements for the free boundary condition ($N = 32$, $t/L = 1/1000$), see Ref. [5] for reference solutions. For the strain calculation, the local Cartesian coordinates '1', '2', and '3' in Fig. 15 are used on the mid-surface of the shell elements, see Fig. 15. The membrane strain components '11', '22' and '12' are normalized by the corresponding maximum bending strain components obtained using the regular 32×32 meshes of MITC4 shell elements. When the regular mesh is used, the membrane strains obtained using both shell elements are quite accurate. For the distorted mesh cases, using the MITC4+ shell element, while not accurately predicting the strains, the given values are much closer to the accurate values of the strains than when using the MITC4 shell element.

7. Concluding remarks

In this study, we developed a new 4-node shell element by alleviating membrane locking. The new assumed strain field was introduced using the membrane strains obtained from triangular subdomains. The MITC4+ shell element passes the isotropy test, zero energy mode test, bending and shearing patch tests, and also very closely the membrane patch test. The MITC4+ shell element shows improved convergence behavior in bending-dominated situations without losing the predictive capability of the membrane behavior compared to the MITC4 shell element. The same approach is also applicable for the 3D-shell element [36].

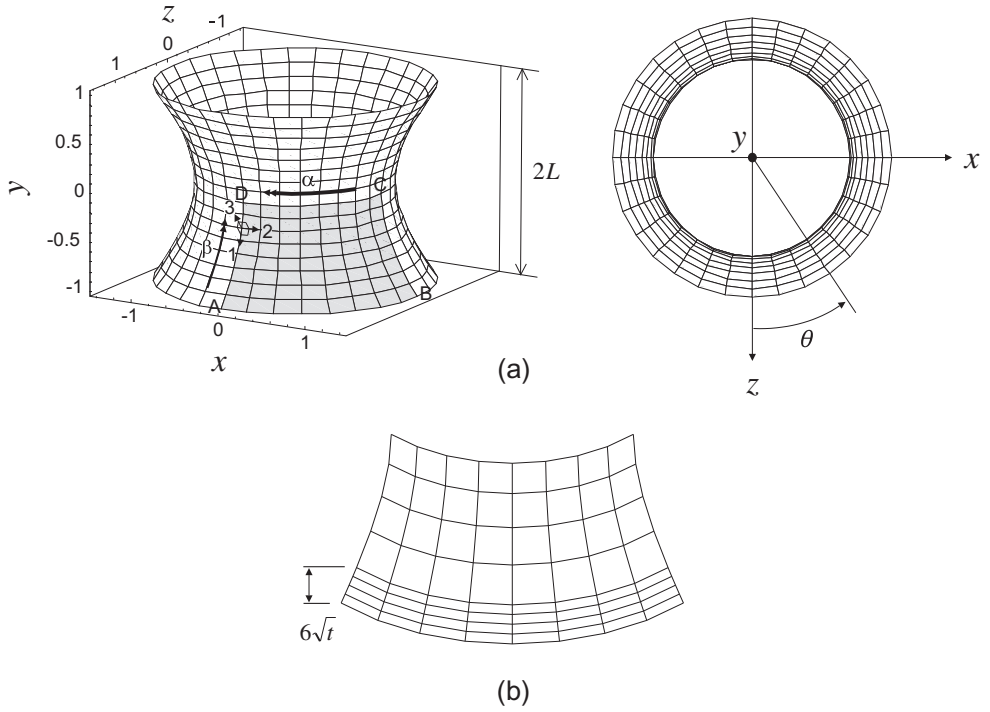

Fig. 15. Hyperboloid shell problem ($E = 2.0 \times 10^{11}$, $\nu = 1/3$ and $p_0 = 1.0$). (a) Problem description. (b) Graded mesh for the clamped case (8×8 mesh, $t/L = 1/1000$).

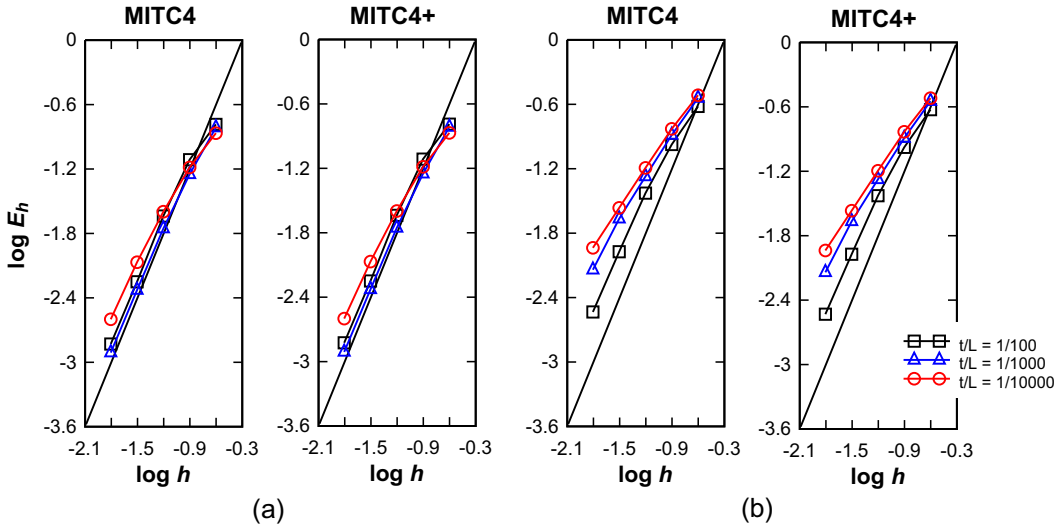

Fig. 16. Convergence curves for the clamped hyperboloid shell problem with (a) the regular and (b) distorted meshes shown in Fig. 10. The bold line represents the optimal convergence rate.

The proposed shell element provides improved performance and some insight into the MITC formulation. However, while the element is useful in engineering analyses, further studies would be necessary to obtain a 4-node quadrilateral shell element that satisfies the basic tests and shows optimal uniform convergence even when highly distorted meshes are employed in the analysis of the hyperboloid shell problems.

Acknowledgments

This work was supported by the Human Resources Development Program (No. 20134030200300) of the Korea Institute of Energy Technology Evaluation and Planning (KETEP) funded by the Ministry of Trade, Industry and Energy, and the National Research Foundation of Korea (NRF) grant funded by the Korea government (MSIP) (No. NRF-2014M2B2A9030561).

Appendix A. Derivation of constants for the center point

We here provide the detailed derivation of Eqs. (8) and (9). As shown in Fig. 4, the geometric centroid of triangle 1 defined by nodes 1–2–4 is

$$\mathbf{x}_{T1} = \frac{1}{3}\mathbf{x}_1 + \frac{1}{3}\mathbf{x}_2 + \frac{1}{3}\mathbf{x}_4 = \begin{bmatrix} \frac{1}{3} & \frac{1}{3} & 0 & \frac{1}{3} \end{bmatrix} \begin{bmatrix} \mathbf{x}_1 & \mathbf{x}_2 & \mathbf{x}_3 & \mathbf{x}_4 \end{bmatrix}^T, \quad \text{(A.1)}$$

and similarly, the geometric centroid of triangle 2 is given by

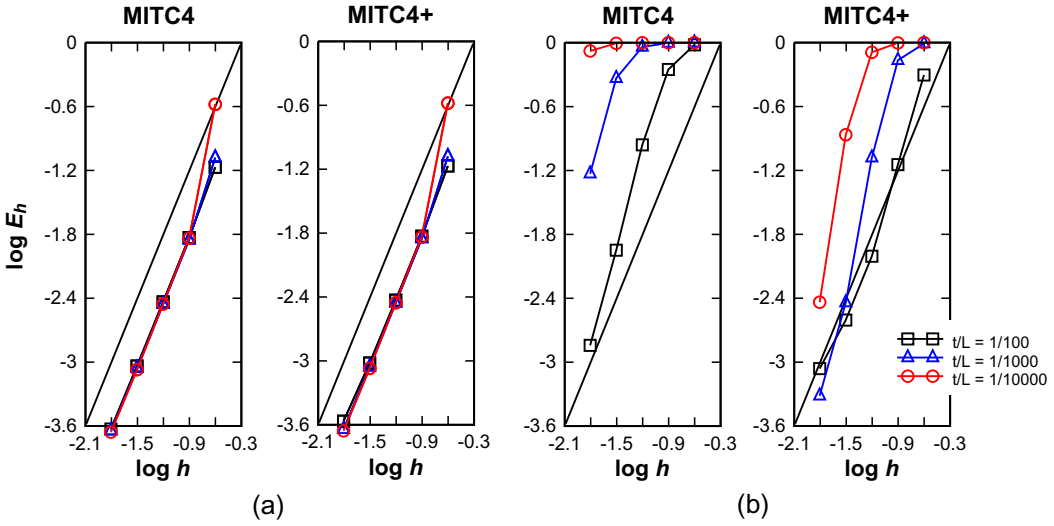

Fig. 17. Convergence curves for the free hyperboloid shell problem with (a) the regular and (b) distorted meshes shown in Fig. 10. The bold line represents the optimal convergence rate.

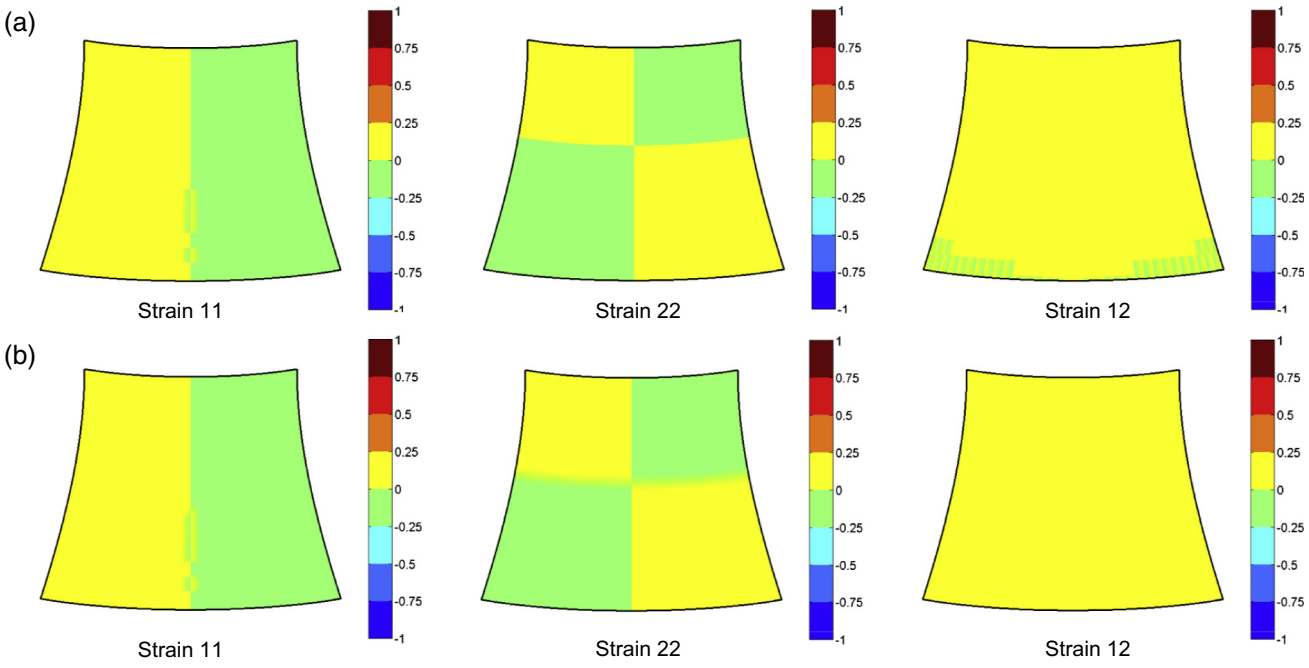

Fig. 18. Membrane strain distributions calculated using the (a) MITC4 and (b) MITC4+ shell elements for the free hyperboloid shell problem with the regular meshes. ($N = 32$, $t/L = 1/1000$.)

$$\mathbf{x}_{T2} = \begin{bmatrix} 0 & \frac{1}{3} & \frac{1}{3} & \frac{1}{3} \end{bmatrix} [\mathbf{x}_1 \quad \mathbf{x}_2 \quad \mathbf{x}_3 \quad \mathbf{x}_4]^T. \tag{A.2}$$

Then, the geometric centroid of triangles 1 and 2 is calculated using the following equation

$$\mathbf{x}_{T12} = \frac{A_1}{A_1 + A_2}\mathbf{x}_{T1} + \frac{A_2}{A_1 + A_2}\mathbf{x}_{T2}, \tag{A.3}$$

where A_1 and A_2 are the areas of triangles 1 and 2 shown in Fig. 4.

Similarly, the geometric centroid of triangles 3 and 4 is

$$\mathbf{x}_{T34} = \frac{A_3}{A_3 + A_4}\mathbf{x}_{T3} + \frac{A_4}{A_3 + A_4}\mathbf{x}_{T4} \tag{A.4}$$

with

$$\mathbf{x}_{T3} = \begin{bmatrix} \frac{1}{3} & \frac{1}{3} & \frac{1}{3} & 0 \end{bmatrix} [\mathbf{x}_1 \quad \mathbf{x}_2 \quad \mathbf{x}_3 \quad \mathbf{x}_4]^T,$$
$$\mathbf{x}_{T4} = \begin{bmatrix} \frac{1}{3} & 0 & \frac{1}{3} & \frac{1}{3} \end{bmatrix} [\mathbf{x}_1 \quad \mathbf{x}_2 \quad \mathbf{x}_3 \quad \mathbf{x}_4]^T,$$

in which A_3 and A_4 are the areas of triangles 3 and 4.

Finally, the mean position of two geometric centroids is simply obtained by

$$\mathbf{x}_5 = \frac{1}{2}(\mathbf{x}_{T12} + \mathbf{x}_{T34}) = [\gamma_1 \quad \gamma_2 \quad \gamma_3 \quad \gamma_4][\mathbf{x}_1 \quad \mathbf{x}_2 \quad \mathbf{x}_3 \quad \mathbf{x}_4]^T = \sum_{i=1}^{4} \gamma_i \mathbf{x}_i \tag{A.5}$$

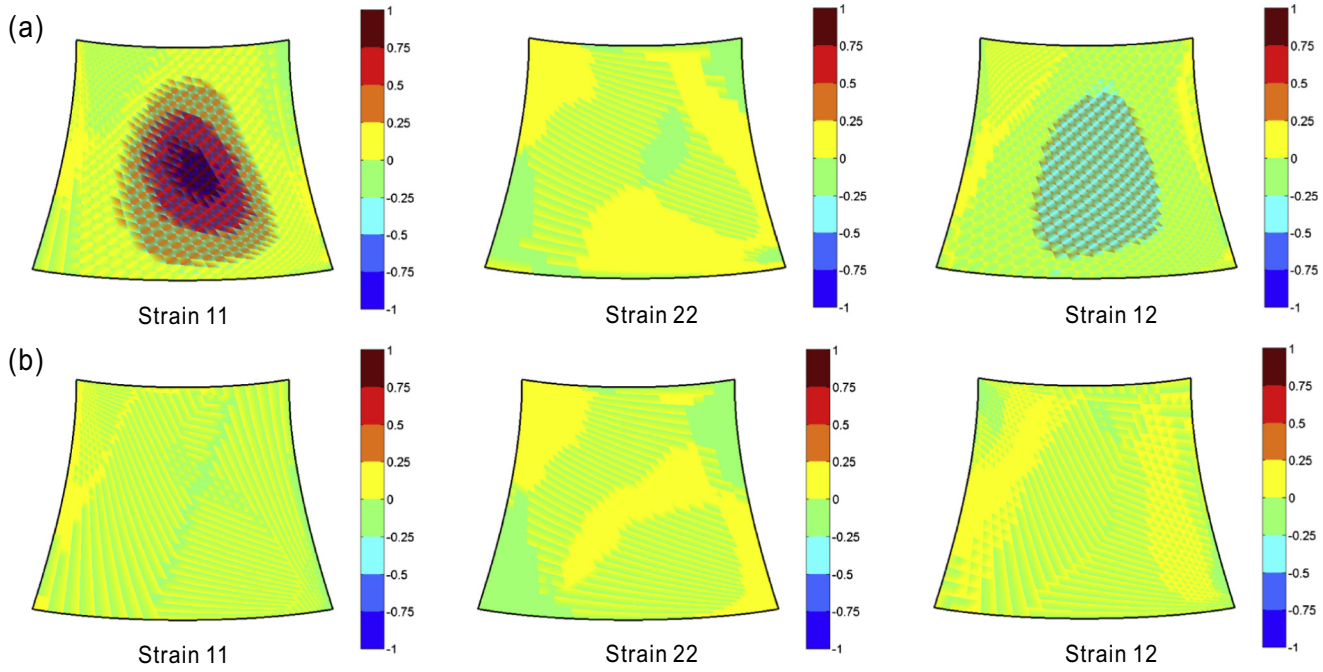

Fig. 19. Membrane strain distributions calculated using the (a) MITC4 and (b) MITC4+ shell elements for the free hyperboloid shell problem with the distorted meshes shown in Fig. 9. ($N = 32$, $t/L = 1/1000$.)

with

$$[\gamma_1 \quad \gamma_2 \quad \gamma_3 \quad \gamma_4] = \frac{1}{2}\frac{A_1}{A_1+A_2}\left[\tfrac{1}{3} \quad \tfrac{1}{3} \quad 0 \quad \tfrac{1}{3}\right] + \frac{1}{2}\frac{A_2}{A_1+A_2}\left[0 \quad \tfrac{1}{3} \quad \tfrac{1}{3} \quad \tfrac{1}{3}\right] + \frac{1}{2}\frac{A_3}{A_3+A_4}\left[\tfrac{1}{3} \quad \tfrac{1}{3} \quad \tfrac{1}{3} \quad 0\right] + \frac{1}{2}\frac{A_4}{A_3+A_4}\left[\tfrac{1}{3} \quad 0 \quad \tfrac{1}{3} \quad \tfrac{1}{3}\right].$$

References

[1] Dvorkin EN, Bathe KJ. A continuum mechanics based four-node shell element for general nonlinear analysis. Eng Comput 1984;1(1):77–88.
[2] Lee PS, Bathe KJ. Development of MITC isotropic triangular shell finite elements. Comput Struct 2004;82(11):945–62.
[3] Lee Y, Lee PS, Bathe KJ. The MITC3+ shell element and its performance. Comput Struct 2014;138:12–23.
[4] Lee Y, Yoon K, Lee PS. Improving the MITC3 shell finite element by using the Hellinger–Reissner principle. Comput Struct 2012;110–111:93–106.
[5] Bathe KJ, Lee PS, Hiller JF. Towards improving the MITC9 shell element. Comput Struct 2003;81(8):477–89.
[6] Bucalem ML, Bathe KJ. Higher-order MITC general shell elements. Int J Numer Meth Eng 1993;36(21):3729–54.
[7] da Veiga LB, Chapelle D, Suarez IP. Towards improving the MITC6 triangular shell element. Comput Struct 2007;85(21):1589–610.
[8] Kim DN, Bathe KJ. A triangular six-node shell element. Comput Struct 2009;87(23):1451–60.
[9] Bathe KJ, Dvorkin EN. A formulation of general shell elements—the use of mixed formulation of tensorial components. Int J Numer Meth Eng 1986;22(3):697–722.
[10] MacNeal RH. Finite elements: their design and performance. Mechanical engineering, vol. 89. New York: Dekker; 1994.
[11] Chapelle D, Bathe KJ. The finite element analysis of shells – fundamentals. Berlin: Springer; 2003 [2nd ed.; 2011].
[12] Bathe KJ. Finite element procedures. Prentice Hall; 1996 [Bathe KJ, 2nd ed. Watertown (MA); 2014].
[13] Chapelle D, Bathe KJ. Fundamental considerations for the finite element analysis of shell structures. Comput Struct 1998;66(1):19–36. 711–2.
[14] Bathe KJ. The inf–sup condition and its evaluation for mixed finite element methods. Comput Struct 2001;79(2):243–52.
[15] Bathe KJ, Iosilevich A, Chapelle D. An inf–sup test for shell finite elements. Comput Struct 2000;75(5):439–56.
[16] Lee PS, Bathe KJ. On the asymptotic behavior of shell structures and the evaluation in finite element solutions. Comput Struct 2002;80(3):235–55.
[17] Bucalem ML, Bathe KJ. Finite element analysis of shell structures. Arch Comput Meth Eng 1997;4(1):3–61.
[18] Prathap G. The finite element method in structural mechanics: principles and practice of design of field-consistent elements for structural and solid mechanics. Dordrecht: Kluwer Academic; 1993.
[19] Bucalem ML, Bathe KJ. Locking behavior of isoparametric curved beam finite elements. Appl Mech Rev 1995;48(11S):S25–9.
[20] Pitkäranta J. The problem of membrane locking in finite element analysis of cylindrical shells. Numer Math 1992;61(1):523–42.
[21] Belytschko T, Tsay CS. A stabilization procedure for the quadrilateral plate element with one-point quadrature. Int J Numer Meth Eng 1983;19(3):405–19.
[22] Belytschko T, Leviathan I. Projection schemes for one-point quadrature shell elements. Comp Meth Appl Mech Eng 1994;115(3):277–86.
[23] Belytschko T, Leviathan I. Physical stabilization of the 4-node shell element with one point quadrature. Comp Meth App Mech Eng 1994;113(3):321–50.
[24] Koschnick F, Bischoff M, Camprubí N, Bletzinger KU. The discrete strain gap method and membrane locking. Comp Meth Appl Mech Eng 2005;194(21):2444–63.
[25] Choi CK, Paik JG. An efficient four node degenerated shell element based on the assumed covariant strain. Struct Eng Mech 1994;2(1):17–34.
[26] Vampa V. Analysis of in-layer strains in the low order MITC shell element. Latin Am J Solid Struct 2007;4(2):87–102.
[27] Dvorkin EN, Vassolo SI. A quadrilateral 2-D finite element based on mixed interpolation of tensorial components. Eng Comput 1989;6:217–24.
[28] Irons BM, Razzaque A. Experience with the patch test for convergence of finite elements. The mathematical foundations of the finite element method with applications to partial differential equations. New York: Academic Press; 1972.
[29] Cook RD. Improved two-dimensional finite element. ASCE J Struct Div 1974;100(9):1851–63.
[30] Simo JC, Rifai MS. A class of mixed assumed strain methods and the method of incompatible modes. Int J Numer Meth Eng 1990;29(8):1595–638.
[31] Bathe KJ, Iosilevich A, Chapelle D. An evaluation of the MITC shell elements. Comput Struct 2000;75(1):1–30.
[32] Hiller JF, Bathe KJ. Measuring convergence of mixed finite element discretizations: an application to shell structures. Comput Struct 2003;81(8):639–54.
[33] Lee PS, Bathe KJ. The quadratic MITC plate and MITC shell elements in plate bending. Adv Eng Softw 2010;41(5):712–28.
[34] Lee PS, Bathe KJ. Insight into finite element shell discretizations by use of the "basic shell mathematical model". Comput Struct 2005;83(1):69–90.
[35] Batoz JL, Bathe KJ, Ho LW. A study of three-node triangular plate bending elements. Int J Numer Meth Eng 1980;15(12):1771–812.
[36] Sussman T, Bathe KJ. 3D-shell elements for structures in large strains. Comput Struct 2013;122:2–12.